Thresholding for Edge Detection in SAR Images

Debashis Sen and Sankar K. Pal
Center for Soft Computing Research, Indian Statistical Institute, 203 B. T. Road, Kolkata, India 700108.
E-mail: {dsen_t, sankar}@isical.ac.in

Abstract- **Selecting a threshold from the gradient histogram, a histogram of gradient magnitudes, of an image plays a crucial role in a gradient based edge detection system. In this paper, we propose a methodology to determine this threshold value when the edge detection system is applied to synthetic aperture radar (SAR) images. We consider a SAR image as a random process, perform a transformation, model the gradient histogram of the transformed image using theories of random process and then determine a region of interest in the gradient histogram using certain properties of a probability density function. Standard histogram thresholding techniques are then used within the region of interest to get the threshold value. The proposed methodology provides a systematic solution to the thresholding problem in gradient based edge detection systems for SAR images and hence results in consistently appreciable performance. Extensive experimental results are shown to demonstrate the effectiveness of the proposed methodology.**

I. Introduction

Synthetic aperture radar (SAR) imaging system, which is used to capture images for purposes such as environmental monitoring, earth-resource mapping and military, has minimum constraints on the time of the day and the atmospheric conditions. The images captured using a SAR imaging system, which is a coherent imaging system, are corrupted by a noise called speckle [1]. In order to reduce the speckle an on-board (built within the capturing system) process called multilook integration is carried out, where incoherent averaging of frames obtained from different segments of the signal frequency spectrum is performed. When L different segments of the signal spectrum are considered, an L-look image is said to be produced [2].

The distribution of the intensity values in a homogenous region of an L-look SAR image can be fairly modeled by a gamma probability density function (PDF) [1]. The lognormal PDF, which is easy to handle statistically, is a very close approximation to the gamma PDF and hence a lognormal PDF can also be considered for the modeling [2, 3]. Edges in an image by intuitive definition are those features which separate various homogenous regions. Therefore, we may model the distributions of two homogenous regions separated by an edge as two lognormal PDFs with different parameters.

A. SAR Images as Random Processes

Considering an image as a random process is intuitively appealing as the gray values at various locations in images obtained using different capturing systems is not deterministic. An image being a random process implies that the gray values at different locations in the image are generated by random variables those characterize the random process. Now, it is obvious that any arbitrary image is of non stationary [4] nature due to the presence of edges. However, we may realistically assume that each region in an image can be represented by a stationary random process [4] preserving the non stationary nature of the overall image. Hence, the gray value at each pixel within a region of an image is generated by a particular random variable, which has a short-tailed probability density function (PDF). The random variable may not have a long-tailed PDF, as such a PDF would imply the presence of abrupt values within a region. An abrupt value in an image should be associated with a pixel of an edge between regions and not with a pixel within a region.

From the earlier explanation about the distribution of intensity values in a homogenous region of an L-look SAR image, we see that the short-tailed PDF mentioned above should be considered as a lognormal PDF and hence the intensity values in various regions of an L-look SAR image would have been generated by a stationary lognormal random process. Therefore, it stands that we represent an L-look SAR image as a wide sense stationary (WSS) [4] mixed lognormal random process. Mixed lognormal random variables, which characterize a SAR (L-look) image ($\overline{X}$), has a PDF of the form

$$f(\overline{X}_{ij}) = \sum_{r=1}^{D} \frac{W_r}{\sqrt{2\pi}\, s_r\, \overline{X}_{ij}} \exp\left(-\frac{(\ln \overline{X}_{ij} - m_r)^2}{2s_r}\right) \qquad (1)$$

where D denotes the number of regions, the weight W_r is the ratio of the area of the r^{th} region to the whole area of the image, m_r and s_r are the mean and standard deviation of the natural logarithm of the samples in the regions, respectively and $\overline{X}_{ij}$ denote the gray values at i^{th} row and j^{th} column of the image $\overline{X}$.

B. Gradient Based Edge Detection System

Among the various edge detection methodologies proposed in literature, the popular are the ones based on finding the gradient magnitudes at each pixel in an image. Such a gradient based edge detection system comprises of a smoothing operation followed by the first-order derivative operation to get the gradient magnitude and direction values at each pixel. Various optimal gradient operators performing the smoothing and first-order derivative operations together have been proposed. The gradient values are then fed to a post processing operation, which usually is an edge thinning operation. One example of such a post processing method is the non-maximum suppression (NMS) proposed in [5], which we consider in this paper.

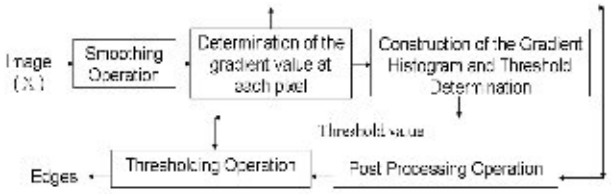

Fig. 1. Gradient based edge detection system

Most of the optimal gradient operators reported in literature are based on the three performance criteria, namely, good detection, good localization and only one response to a single edge, given by Canny [5]. The optimizations of these three criteria are contradictory and hence a trade-off is required. Such a trade-off implies that the smoothing operation cannot remove the "false" edges due to the noise and inherent texture completely. Hence, after all the operations mentioned above, we need a decision making system in order to distinguish the actual edges from the "false" edges. This decision making system, in general, is a thresholding operation with the threshold being determined from the histogram of gradient magnitudes (gradient histogram). A block diagram of the gradient based edge detection system is given in Fig. 1.

Considering the criticality of the thresholding process in the overall edge detection system, it is surprising that except for a few researchers [6-8], no one else has addressed this problem of gradient histogram thresholding to the best knowledge of the authors. In [6], the gradient histogram was assumed to be a weighted sum of two gamma densities in order to identify a threshold by parameter estimation. However, no justification was given for such an assumption. In [7], a cubic facet model for image and a Gaussian model for noise were considered and various parameters were estimated in order to determine the threshold using the Bayes decision procedure. Such a method is very complex and apart from the error in the decision, the edge detection performance also depends on the modeling error. In [8], the author considers that gradient histograms are unimodal in nature and hence propose a unimodal thresholding algorithm that finds a corner in the histogram.

In this paper, we propose a methodology to determine a threshold from the gradient histogram in order to separate the actual (desired) edges in a SAR image from the "false" edges using the "prior" knowledge about the distribution of the intensity values in its homogenous regions. Natural logarithm is first applied on the SAR image to get a transformed image. A region of interest (ROI) in the gradient histogram of the transformed image is then obtained by computing certain skewness and kurtosis values and comparing them to some predefined constants. These constants are determined by approximately modeling a gradient histogram using various theories of random processes. Once the ROI in the gradient histogram has been obtained, any general histogram thresholding algorithm could be applied to the ROI in order to determine the threshold value. We consider, for example, the histogram thresholding algorithms given in [9] and [10]. The threshold thus obtained is taken as the upper threshold for the hysteresis process [5], which is applied on the output from the NMS operation to get the edges in the transformed image. Note that the application of natural logarithm on images does not affect any desired property of the edges. Hence, the edges found in the transformed image would correspond to the edges in the SAR image. The effectiveness of the proposed methodology is demonstrated using a few SAR images. A very interesting aspect of the proposed method of threshold determination is that it is applicable to gradient histograms obtained after the application of any linear gradient operator.

The organization of the paper is as follows. Section II and III describes the gradient histogram modeling and threshold determination, respectively. Experimental results are given in Section IV and the paper concludes with Section V outlining the contributions made.

II. Gradient Histogram Modeling

In this section, we shall model the gradient histogram of an image, say X, which can be represented by a WSS mixed Gaussian random process. Note that it is always appropriate to model any arbitrary (no "prior" knowledge) image using a mixed Gaussian random process. Such a model implies that the distribution of the intensity value in homogenous regions of the image is Gaussian, which is suitable as a Gaussian PDF is a short-tailed PDF (See Section I). However, as mentioned earlier, an L-look SAR image ($\overline{X}$) is represented by a WSS mixed lognormal random process. Hence, we need to apply a natural logarithmic transformation logarithmic transformation on the pixels of $\overline{X}$ before the gradient based edge detection system is used. Hence, we have

$$X_{ij} = \ln(\overline{X}_{ij}) \tag{2}$$

Note that X_{ij} and $\overline{X}_{ij}$ are time samples of random processes and hence they are random variables.

A. Linear Gradient Operators

Various gradient operators for edge detection proposed by different authors [5, 11-13] after optimizing various criteria are linear in nature or can be very closely approximated by a linear operator. The application of any linear gradient operator (H) on a digital image (X) can be represented by a window operation such as

$$Y_{ijg} = \sum_{p} \sum_{q} H_{pqg} X_{i+pj+q} \tag{3}$$

where $p = -k, \cdots, 0, \cdots, +k$ and $q = -k, \cdots, 0, \cdots, +k$. In the above, $(2k+1)\times(2k+1)$ gives the size of the window, otherwise referred to as the width of the operator. The symbol g indicates the direction of operation on an image, that is, the horizontal (R) and vertical (C) directions in which the gradient is determined. It is obvious that the vertical component Y_{ijR} and the horizontal component Y_{ijC} of

the gradient are orthogonal to each other. The magnitude of the gradient at each pixel in the image is obtained by

$$G_{ij} = \sqrt{(Y_{ijR})^2 + (Y_{ijC})^2} \tag{4}$$

The image G of gradient magnitudes can be represented by a WSS random process. This is due to the reason that both Y_R and Y_C are WSS mixed Gaussian random processes as a WSS mixed Gaussian random process to a linear system produces another mixed Gaussian WSS random process [4].

Modeling the gradient histogram, say $h(G)$, now boils down to the determination of the PDF of G_{ij}. However, in order to find the PDF of G_{ij}, we require the joint PDF of Y_{ijR} and Y_{ijC}. We know that Y_{ijR} and Y_{ijC} are individually mixed Gaussian distributed and as they are obtained by applying the same mixed Gaussian random process X to different linear systems, they are mutually dependent. Let us now consider a random variable A, such that

$$A = aY_{ijR} + bY_{ijC} \tag{5}$$

where a and b are arbitrary real-valued constants. The random variable A is mixed Gaussian distributed as both Y_{ijR} and Y_{ijC} have been obtained by a linear operation on the same set of various random variables which are individually and jointly mixed Gaussian distributed. The random variable A being mixed Gaussian distributed implies that Y_{ijR} and Y_{ijC} has a bivariate mixed Gaussian PDF [4]. Note that it can be easily shown that a bivariate mixed Gaussian PDF is in fact a mixed bivariate Gaussian PDF. Therefore, the joint PDF of Y_{ijR} and Y_{ijC} is given as

$$f(Y_{ijR}, Y_{ijC}) = \sum_{r_G} \frac{\omega_{r_G}}{2\pi\nu_{1r_G}\nu_{2r_G}\sqrt{1-\rho_{r_G}^2}} \exp\left(-\frac{1}{2(1-\rho_{r_G}^2)}\left(\frac{(Y_{ijR}-\mu_{1r_G})^2}{\nu_{1r_G}^2} + \frac{(Y_{ijC}-\mu_{2r_G})^2}{\nu_{2r_G}^2} - 2\rho_{r_G}\frac{(Y_{ijR}-\mu_{1r_G})(Y_{ijC}-\mu_{2r_G})}{\nu_{1r_G}\nu_{2r_G}}\right)\right) \tag{6}$$

where r_G represents all the regions corresponding to Y_{ijR} and Y_{ijC}, μ_{1r_G} and ν_{1r_G} are the means and standard deviations corresponding to Y_{ijR}, and μ_{2r_G} and ν_{2r_G} are the means and standard deviations corresponding to Y_{ijC}. The ω_{r_G} are certain constant weights. Now, as mentioned earlier, Y_{ijR} and Y_{ijC} are orthogonal to each other. Therefore, the correlation between Y_{ijR} and Y_{ijC} is zero, that is $R_{Y_{ijR}Y_{ijC}} = 0$. Hence, the correlation co-efficient between Y_{ijR} and Y_{ijC} is given by

$$\rho = -\frac{\mu_1\mu_2}{\nu_1\nu_2} = -\frac{\mu_1\mu_2}{\sqrt{(\mathrm{M}_1-\mu_1^2)(\mathrm{M}_2-\mu_2^2)}} \tag{7}$$

where μ_1 and μ_2 are the first order moments of Y_{ijR} and Y_{ijC}, respectively, M_1 and M_2 are the second order moments and ν_1 and ν_2 are the standard deviations. We have

$$\mu_1 = \sum_{r_1} \upsilon_{1r_1}\mu_{1r_1}, \mathrm{M}_1 = \sum_{r_1} \upsilon_{1r_1}\mathrm{M}_{1r_1},$$
$$\mu_2 = \sum_{r_2} \upsilon_{2r_2}\mu_{2r_2}, \mathrm{M}_2 = \sum_{r_2} \upsilon_{2r_2}\mathrm{M}_{2r_2} \tag{8}$$

where r_1 and r_2 respectively represent the regions corresponding to Y_{ijR} and Y_{ijC}, and υ_{1r_1} and υ_{2r_2} are the weights corresponding to the random variables Y_{ijR} and Y_{ijC}, respectively. The constants ω_{r_G} in (6) are formed from the various products of υ_{1r_1} and υ_{2r_2}. From (8), we see that the first (mean) and second order moments of Y_{ijR} and Y_{ijC} are the weighted sums of the first (mean) and second order moments of the constituent Gaussian functions.

We shall now consider a few aspects of an image and the modeling of each region in an image using a Gaussian process and then the whole image as a mixed Gaussian process, in order to explore the nature of the joint PDF given in (6).

First, let us consider a few realistic aspects of an image. In general, the edges in an image cover much less area in the scene than the homogeneous regions. Hence the weighting constants υ_{1r_1} and υ_{2r_2} corresponding to those values of r_1 and r_2 when $\mu_{1r_1} \approx 0$ and $\mu_{2r_2} \approx 0$ would be much larger than the others. It can also be realistically assumed that among μ_{1r_1} and μ_{2r_2} for other values of r_1 and r_2, some would have negative values and some would have positive. Hence, the values of μ_1 and μ_2 would be very near to zero. On the other hand, as M_1 and M_2 indicate the "amount" of texture present in various regions, their values would not be small compared to μ_1 and μ_2. Hence, we may conclude from the expression in (7) that the value of ρ would be very small and might be considered negligible (zero). As Y_{ijR} and Y_{ijC} are mixed Gaussian distributed, a small value of ρ suggests that the random variables Y_{ijR} and Y_{ijC} are weakly dependent on each other. Now, as the weighting constants ω_{r_G} are products of various υ_{1r_1} and υ_{2r_2}, they would be large for those values of r_G when $\mu_{1r_G} \approx 0$ and $\mu_{2r_G} \approx 0$ compared to others. Hence, we may consider that the values of ρ_{r_G} are small in general. Note that r_G denotes all combinations of r_1 and r_2.

Secondly, we have considered that each region of an image X, which is subjected to the gradient operator, is generated by a Gaussian process and thus the whole image is generated by a mixed Gaussian process. The values of the random variables Y_{ijR} and Y_{ijC} are obtained by performing a weighted summation operation (see (3)) on the same set of pixels of the input image and hence they would have the same value of variance [4], that is, $\nu_1 = \nu_2$. Now as each value of Y_{ijR} and Y_{ijC}, that is the value at a particular pixel in these two gradient images, is generated uniquely from a single Gaussian function among all the Gaussian function in the expressions of the mixed Gaussian PDF, we deduce that the expression in (6) would not have any term such that $\nu_{1r_G} \neq \nu_{2r_G}$. Hence, we shall always have $\nu_{1r_G} = \nu_{2r_G} = \nu_{r_G}$.

Let us now consider the following expression

$$f_a(Y_{ijR}, Y_{ijC}) = \sum_{r_G} \frac{\omega_{r_G}}{2\pi\nu_{1r_G}\nu_{2r_G}} \exp\left(-\frac{1}{2}\left(\frac{(Y_{ijR}-\mu_{1r_G})^2}{\nu_{1r_G}^2} + \frac{(Y_{ijC}-\mu_{2r_G})^2}{\nu_{2r_G}^2}\right)\right) \tag{9}$$

Note that the above equation has been obtained by substituting $\rho_{r_G} \approx 0$ in (6). Now, as we have found that the correlation co-efficient between Y_{ijR} and Y_{ijC} is very small and the values of ρ_{r_G} (see (6)) are small in general, we may approximately consider that Y_{ijR} and Y_{ijC} are mutually independent. Therefore we may realistically assume that $f(Y_{ijR}, Y_{ijC}) \approx f_a(Y_{ijR}, Y_{ijC})$.

Now considering $f_a(Y_{ijR}, Y_{ijC})$, we shall find the PDF of G_{ij}. According to [4], the PDF of G_{ij} is given by

$$f(G_{ij}) \approx \int_{-G_{ij}}^{G_{ij}} \frac{G_{ij}}{\sqrt{G_{ij}^2 - Y_{ijC}^2}} [f_a(\sqrt{G_{ij}^2 - Y_{ijC}^2}, Y_{ijC}) + f_a(-\sqrt{G_{ij}^2 - Y_{ijC}^2}, Y_{ijC})] dY_{ijC} \quad (10)$$

Substituting the expression of f_a in (9), we arrive at

$$f(G_{ij}) \approx \sum_{r_G} \omega_{r_G} \left(\frac{G_{ij} \exp\left(-\frac{G_{ij}^2 + \sqrt{\mu_{1r_G}^2 + \mu_{2r_G}^2}}{2\nu_{r_G}^2}\right)}{\nu_{r_G}^2} \times \mathbf{I}_0\left(\frac{G_{ij}\sqrt{\mu_{1r_G}^2 + \mu_{2r_G}^2}}{\nu_{r_G}^2}\right)\right) \quad (11)$$

where $\mathbf{I}_0$ is the zeroth order modified Bessel function of the first kind. The random variable G_{ij} represents the magnitude of the gradient present at the $(i, j)^{\text{th}}$ position of the image under consideration. As we can see from (11) the PDF of G_{ij} is approximately a weighted sum of Rician PDFs [14]. Now, consider the case when $\mu_{1r_G} \approx 0$ and $\mu_{2r_G} \approx 0$, that is, the homogeneous areas (A_H) in the image. Then we have

$$f(G_{ij})_{A_H} \approx \sum_{r_G \in A_H} \omega_{r_G} \times \frac{G_{ij} \exp\left(-\frac{G_{ij}^2}{2\nu_{r_G}^2}\right)}{\nu_{r_G}^2} \quad (12)$$

Hence, the PDF of G_{ij} representing the magnitude of gradient at locations in the homogeneous areas of the image is a weighted sum of Rayleigh PDFs. Note that the Rayleigh PDF is a special case of the Rician PDF. The value of ν_{r_G} indicates the variation of the random texture in a region. In an image, this variation is considerably less than the difference in the means of any two regions separated by an edge. Therefore, in the areas of the image containing edges (A_E), we shall have $\sqrt{\mu_{1r_G}^2 + \mu_{2r_G}^2} \gg \nu_{r_G}$. We find that in

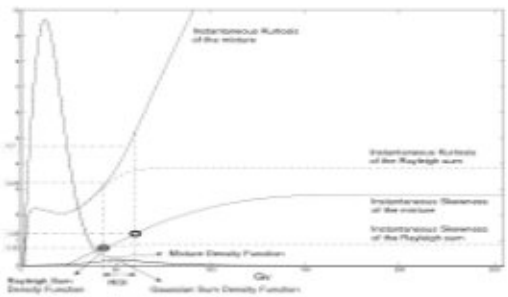

Fig. 2. Separation of a weighted sum of Rayleigh and a weighted sum of Gaussian PDFs using instantaneous skewness and kurtosis values of their mixture and the determination of the ROI.

such cases, the PDF of G_{ij} is given by a weighted sum of Gaussian PDFs as shown below.

$$f(G_{ij})_{A_E} \approx \sum_{r_G \in A_E} \omega_{r_G} \times \exp\left(-\frac{(G_{ij} - \sqrt{\mu_{1r_G}^2 + \mu_{2r_G}^2})^2}{2\nu_{r_G}^2}\right) \quad (13)$$

Hence, we see that every Rician PDF in (11) reduces either to a Rayleigh PDF or to a Gaussian PDF in our analysis. Now, the whole image is given by the accumulation of A_H and A_E. Hence, we have an approximate model for a gradient histogram of an image as $h(G) \approx f(G_{ij}) = f(G_{ij})_{A_H} + f(G_{ij})_{A_E}$.

III. Region of Interest and Threshold Determination

From the analysis in the previous section, we deduce that in order to obtain the edges in an image and remove the "false" edges due to inherent texture and noise, we need a threshold value to distinguish and separate $f(G_{ij})_{A_H}$ and $f(G_{ij})_{A_E}$ given the $h(G)$ of a particular image. In other words, we need to distinguish between the components (bins indicating the number of occurrences) of the gradient histogram ($h(G)$) given by the expression of the weighted sum of Rayleigh PDFs and the weighted sum of Gaussian PDFs.

In order to distinguish the components of $h(G)$, we shall consider skewness and kurtosis values as for a Rayleigh and a Gaussian PDF, skewness and kurtosis are constants which do not vary with the parameters of the density function. The expressions of skewness (S) and kurtosis (K) [4] are

$$S = \frac{\Theta_3}{\Theta_2^{3/2}} \quad (14)$$

$$K = \frac{\Theta_4}{\Theta_2^2} \quad (15)$$

where Θ_n stands for n^{th}-order central moment corresponding to the PDF of the random variable under consideration. For a Rayleigh PDF, we have, $S \approx 0.63$ and $K \approx 3.25$ and for a Gaussian PDF $S = 0$ and $K = 3$.

In order to carry out the desired separation, we calculate the instantaneous skewness ($S(G_v)$) or kurtosis ($K(G_v)$) of $h(G)$ progressing along the increasing values of gradient magnitude G_v (see Fig. 2). That is, $S(G_v)$ and $K(G_v)$ for $h(G)$ respectively give the skewness and kurtosis values for the data represented by all those bins of $h(G)$ where the gradient magnitude value is less than G_v. We shall then set that G_v value as threshold where the skewness or kurtosis first respectively equals the skewness or kurtosis values of a weighted sum of Rayleigh PDFs. However, determination of skewness or kurtosis values of a weighted sum of Rayleigh PDFs is a non-trivial task. Let us consider the following expression

$$V(\varpi) = \int_0^t \frac{\varpi}{\vartheta^2} \exp\left(-\frac{\varpi^2}{2\vartheta^2}\right) d\vartheta = \sqrt{2\pi}\left(\frac{1}{2} - \text{erf}\left(\frac{\varpi}{t}\right)\right) \quad (16)$$

The above expression gives the sum of an infinite number of Rayleigh PDFs. We calculate the skewness (S) and kurtosis (K) of $V(\varpi)$ given by (16) and obtain $S \approx 1.25$

and $K \approx 4.7$. Hence, the skewness and kurtosis values of a sum of a large number of Rayleigh PDFs do not vary with the underlying parameters. We empirically determine that when the number of Rayleigh PDFs in the weighted sum is not large $S < 1.25$ and $K < 4.7$ .Hence, we may consider $S \approx 1.25$ and $K \approx 4.7$ respectively as the maximum values of the skewness and kurtosis that a weighted sum of Rayleigh PDFs can have. Note that although we now know the range of values that the skewness and kurtosis measures of a sum of Rayleigh PDFs may take, we remain devoid of knowing the actual values a particular sum of Rayleigh PDFs would take.

Consider the expression in (12). We see that if we come across an image for which all v_{r_G} are equal or there is only one homogeneous region in the image, then the weighted sum of the Rayleigh PDFs will reduce to a single Rayleigh PDF. Hence, we shall consider that value of G_v as the threshold where we get $S(G_v) = .63$ or $K(G_v) = 1.25$. On the other hand, in some other image we might have a large number of objects with texture such that all v_{r_G} are different. In such a case, the weighted sum of Rayleigh PDFs will contain a large number of Rayleigh PDFs and hence we shall consider that value of G_v as the threshold, where $S(G_v) = 3.25$ or $K(G_v) = 4.7$.

Therefore, given a gradient histogram $h(G)$, we may define a Region of Interest (ROI) within which the threshold value would lie. This ROI contains all the components of $h(G)$ starting from the G_v when $S(G_v) = 0.63$ or $K(G_v) = 1.25$ until the value of G_v when $S(G_v) = 1.25$ or $K(G_v) = 4.7$. Note that use of skewness or kurtosis may produce different ROIs as the amount of decision error may not be the same for both the cases. In this paper, we shall use both the skewness and kurtosis based approaches and define the ROI from the smallest G_v to the largest G_v among the four values obtained (see Fig. 2).

A. Threshold determination and post-processing

From the analysis presented till now, we have approximately obtained a ROI in the gradient histogram $h(G)$ where the required threshold would lie. In order to find a single threshold value T to eliminate the "false" edges, we now need to consider only the components in the ROI and not the overall gradient histogram $h(G)$.

After the ROI in the gradient histogram is obtained, we suggest that any conventional histogram thresholding algorithm may be used on the components in the ROI in order to determine the threshold T . In our experiment (see Section IV), we consider the two histogram thresholding algorithms, namely, Otsu's method [9] and beam theory based method [10], as examples, to be used on the components in the ROI. As mentioned earlier, once the threshold T has been obtained from the gradient histogram $h(G)$, we carry out a few post-processing tasks in order to get the edges in the image under consideration. The post-processing tasks used are the non-maximum suppression (NMS) and the hysteresis thresholding. In the NMS operation, which is applied on the image of gradient magnitudes G , it is considered that an edge at a pixel is legitimate only when the gradient magnitude at that pixel assumes a maximum along the gradient direction in a local neighborhood [5]. The hysteresis thresholding process, which is applied on the image obtained at the output of the NMS operation, employs two different thresholds, namely, the upper and the lower threshold [5]. We consider the threshold found by the proposed methodology as the upper threshold and the lower threshold as the upper threshold multiplied by 0.4. Hysteresis thresholding is used as it is highly successful in dealing with the detrimental edge streaking problem.

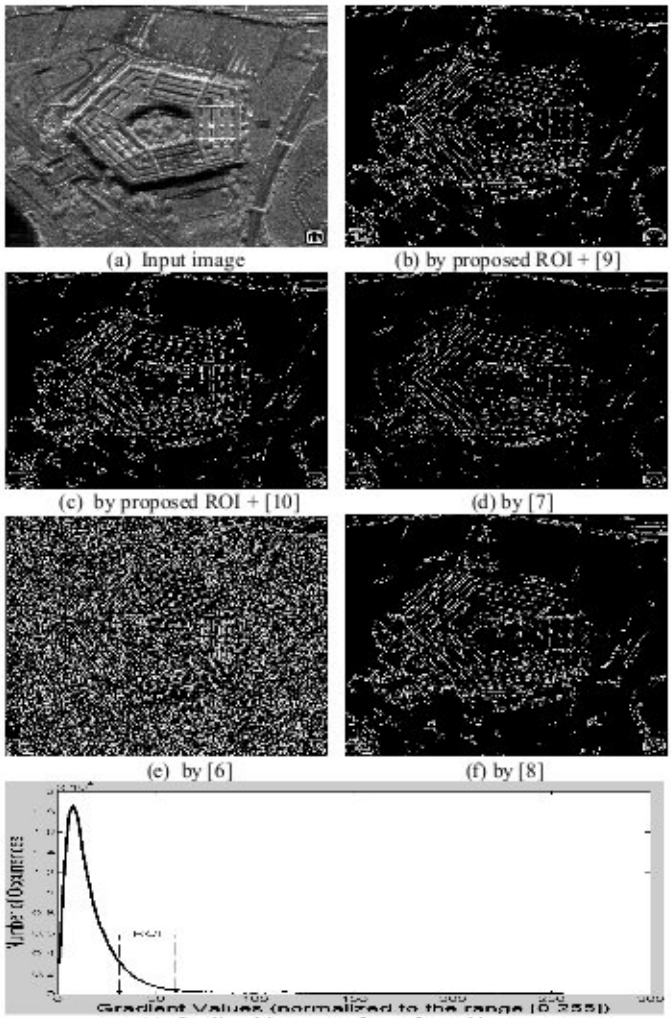

(a) Input image (b) by proposed ROI + [9]
(c) by proposed ROI + [10] (d) by [7]
(e) by [6] (f) by [8]
(g) Gradient histogram of transformed image

Fig. 3. Edges in a SAR image obtained using Canny's gradient operator, the various gradient histogram thresholding techniques and the mentioned post-processing operations

IV. Experimental Results

In this Section, we provide experimental results using two SAR images in order to demonstrate the superiority of the

proposed methodology over the others. The existing techniques to perform gradient histogram thresholding considered for comparison are the ones proposed in [6], [7] and [8]. Note that, to the best knowledge of the authors, there exists no other thresholding technique intended for gradient histograms. Qualitative evaluation of performance is considered in this paper. Quantitative evaluation is avoided as there is no globally accepted objective measure present for evaluating the thresholding process for edge detection.

A SAR image of the famous pentagon building in U. S. A is shown in Fig. 3. The gradient histogram shown in Fig. 3(g), which is considered for threshold determination, is that of the transformed image. We see that the technique proposed by [6] fails to remove the "false" edges due to texture and noise. Although the other existing techniques give satisfactory results, the proposed ones outperform all the others in reducing "false" edges and also in extracting the appropriate edges.

Fig. 4 demonstrates the usage of the proposed thresholding technique with different linear gradient operators, namely, Canny's step edge detecting operator [5], Petrou's ramp edge detecting operator [13] and Sobel's operator [15] on a SAR image of an agricultural region. Note that Sobel's operator is not an optimal operator unlike the other two. It is evident from the figure that although the usage of an appropriate linear gradient operator is crucial for edge detection, the proposed thresholding technique gives acceptable results with any linear gradient operator.

It is extremely difficult to claim or prove that a thresholding technique would always give better results than any other. However, the consistency of a thresholding technique in providing acceptable results is extremely important. We have considered many images of widely different types and applied gradient based edge detection systems using our methodology of threshold determination. The edge detection results obtained in all have been found highly satisfactory. We are unable to report more results in this paper due to lack of space.

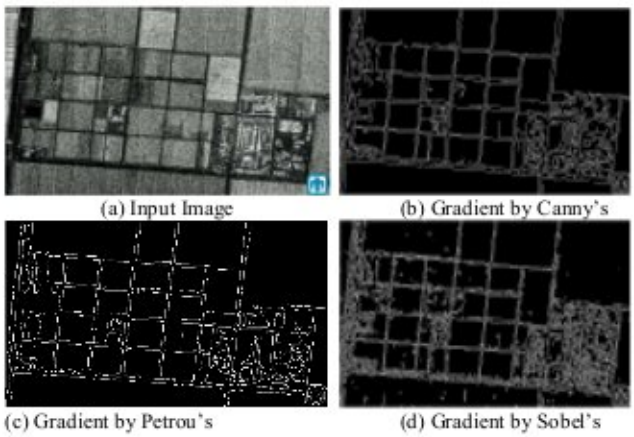

(a) Input Image (b) Gradient by Canny's

(c) Gradient by Petrou's (d) Gradient by Sobel's

Fig. 4. Edges obtained using different linear gradient operators, the proposed thresholding technique of determining an ROI and then using [9], and the mentioned post-processing operations

V. Conclusion

A methodology of thresholding for edge detection in a SAR image has been proposed in this paper. The proposed methodology has been systematically obtained based on certain realistic assumptions and "prior" knowledge about a SAR image. Theories of random process have been considered here to perform a transformation on the SAR image and deduce a general model for a gradient histogram of the transformed image. Certain properties of a probability density function have been used to determine a region of interest (ROI) in the gradient histogram, from which the threshold value has been obtained using standard histogram thresholding techniques. Experiments have been carried out using a few SAR images and different gradient operators. It has been observed that the use of the concept of ROI on edge detection systems helps in consistently obtaining appreciable performance. Moreover, the proposed methodology is seen to score over the few existing techniques of the same paradigm in extracting both the appropriate edges from SAR images and removing the unwanted due to inherent texture and noise.

References

[1] J. W. Goodman, *Speckle Phenomenon in Optics: Theory and Applications*, Roberts and Company, Denver, CO, USA, Sept, 2006.

[2] D. Sen, M. N. S. Swamy and M. O. Ahmad, "Unbiased homomorphic system and its application in reducing multiplicative noise," *IEE Proceedings: Vision, Image and Signal Processing*, vol. 153, no. 5, pp. 521-537, 2006.

[3] L. Gagnon and A. Jouan, "Speckle filtering of SAR images- a comparative study between complex wavelet-based and standard filters," *SPIE Proc.* #3169, pp. 80-91, 1997.

[4] A. Papoulis and S. U. Pillai, *Probability, Random Variable and Stochastic Processes*, 4th ed. McGraw-Hill, 2001.

[5] J. Canny, "A computational approach to edge detection," *IEEE Trans. Pattern Anal. Machine Intell*, vol. 8, no. 6, pp. 679–698, 1986.

[6] P. V. Henstock and D. M. Chelberg, "Automatic gradient threshold determination for edge detection," *IEEE Trans. Image Processing*, vol. 5, no. 5, pp. 784–787, 1996.

[7] O. A. Zuniga and R. M. Haralick, "Gradient threshold selection using the facet model," *Pattern Recognition*, vol. 21, no. 5, pp. 493–503, 1988.

[8] P. L. Rosin, "Unimodal thresholding," *Pattern Recognition*, vol. 34, no. 11, pp. 2083–2096, 2001.

[9] N. Otsu, "A threshold selection method from gray-level histogram," *IEEE Trans. Syst., Man, Cybern.*, vol. 9, no. 1, pp. 62–66, 1979.

[10] D. Sen and S. K. Pal, "Histogram thresholding using beam theory and ambiguity measures," *Fundamenta Informaticae*, vol. 75, no. 1-4, pp. 483–504, 2007.

[11] J. Shen and S. Castan, "An optimal linear operator for step edge detection," *Graphical Models and Image Processing*, vol. 54, no. 2, pp. 112–133, 1992.

[12] S. Sarkar and K. L. Boyer, "On optimal infinite impulse response edge detection filters," *IEEE Trans. Pattern Anal. Machine Intell.*, vol. 13, no. 11, pp. 1154–1171, 1991.

[13] M. Petrou and J. Kittler, "Optimal edge detectors for ramp edges," *IEEE Trans. Pattern Anal. Machine Intell.*, vol. 13, no. 5, pp. 483–491, 1991.

[14] S. O. Rice, "Mathematical analysis of random noise," *Bell System Technical Journal*, vol. 24, pp. 46–156, 1945.

[15] I. E. Sobel, "Camera model and machine perception," *Ph.D. dissertation*, Standford University, 1970.